Structure-Activity Relationship of Benzophenazine Derivatives for Homogeneous and Heterogenized Photooxygenation Catalysis

Nathalie Body,[a] Corentin Lefebvre,[a] Sarah Eeckhout,[a] Anne-Sophie Léonard,[a] Ludovic Troian-Gautier,[a] Sophie Hermans[a] and Olivier Riant[a]**

[a] Université catholique de Louvain (UCLouvain), Institut de la Matière Condensée et des Nanosciences (IMCN), Molecular Chemistry, Materials and Catalysis (MOST), Place Louis Pasteur 1, bte L4.01.02, 1348 Louvain-la-Neuve, Belgium

*Correspondence to: sophie.hermans@uclouvain.be; olivier.riant@uclouvain.be

ABSTRACT

Singlet oxygen is a powerful oxidant used in various applications, such as organic synthesis, medicine, and environmental remediation. Organic and inorganic photosensitizers are commonly used to generate this reactive species through energy transfer with the triplet ground state of oxygen. We describe here a series of novel benzophenazine derivatives as a promising class of photosensitizers for singlet oxygen photosensitization. In this study, we investigated the structure-activity relationship of these benzophenazine derivatives. Akin to a molecular compass, the southern fragment was first functionalized with either aromatic tertiary amines, alkyl tertiary amines, aromatic sulfur groups, alkyl sulfur groups, or cyclic ethers. Enhanced photophysical properties (in terms of triplet excited-state lifetime, absorption wavelength, triplet state energy, and O_2 quenching capabilities) were obtained with cyclic ether and sulfur groups. Conversely, the presence of an amine moiety was detrimental to the photocatalysts. The western and northern fragments were also investigated and slightly undesirable to negligible changes in photophysical properties were observed. The most promising candidate was then immobilized on silica nanoparticles and its photoactivity was evaluated in the citronellol photooxidation

reaction. A high NMR yield of 97 % in desired product was obtained, with only a slight decrease over several recycling runs (85 % in the fourth run). These results provide insights into the design of efficient photosensitizers for singlet oxygen generation and the development of heterogeneous systems.

TOC GRAPHICS

A new familly of benzophenazine derivatives was designed as photosensitizers for singlet oxygen generation. Extensive structure activity relationship was carried out using both experimental and theoretical approach. The most promising candidate was immobilized on silica nanoparticles and its photoactivity was evaluated in the citronellol photooxidation.

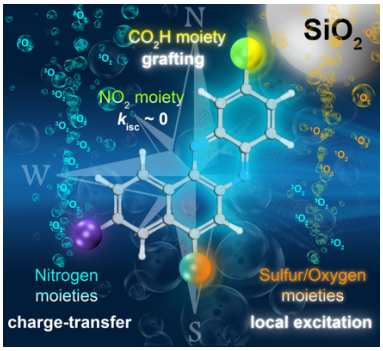

Institute and/or researcher Twitter name: @C_unelma, @LudoTroian, @SophieHermans6, @OlivierRiant

KEYWORDS

Singlet oxygen, Substitution, Silica nanoparticles, Recyclability, Photosensitization, Energy Transfer.

1. INTRODUCTION

Dioxygen (O_2) molecules participate actively in the earth's atmospheric chemistry and in diverse chemical and biological processes.[1] Indeed, naturally occurring triplet dioxygen is necessary for the anabolism of aerobic living beings whereas other reactive oxygen species (ROS) are involved in cell damage leading to organism aging and the development of cancers.[2] ROS are photogenerated according to two mechanisms. The type I mechanism involves hydrogen-atom abstraction or an electron transfer between an excited photosensitizer (PS) (9,10-dicyano anthracene – DCA for example) and a substrate (such as electron-rich alkenes), yielding free radicals that react with oxygen to produce ROS, such as the superoxide radical anion. In the type II mechanism, an energy transfer takes place between an excited photosensitizer and triplet oxygen, forming singlet oxygen ($^1O_2$).[2b, 3]

Singlet oxygen is a powerful reactant with many applications in the environmental domain where it can be used for water disinfection[4] or pollutant degradations,[5] in medicine for photodynamic therapy[6] and bacterial disinfection,[7] or even in organic synthesis for photooxidations reactions.[8] Such

oxidations are applied at industrial scale for the production of rose oxide developed by Symrise company[9] or the photooxygenation of dihydroartemisinic acid in the synthesis of artemisinin implemented by Sanofi.[10]

Singlet oxygen can be easily photogenerated through a type II mechanism using photosensitizers which, by absorption of light, are excited to their singlet state S_1 (**Scheme 1**). An efficient intersystem crossing (ISC) is a prerequisite to forming the corresponding triplet state T_1 that is then able to transfer energy to the ground-state triplet oxygen. The ground state photosensitizer is therefore recovered while $^1O_2$ is formed.[9] Diverse (metal-)organic photosensitizers have shown singlet oxygen generating ability. Transition metal complexes based on ruthenium,[11] iridium,[12] or even copper[13] centers are potential candidates but the use of organic dyes is predominant. Among them, xanthenes (Rose Bengal (RB), eosin Y),[14] phenothiazines (methylene blue),[8b, 15] tetrapyrroles (porphyrins, phthalocyanines, chlorins, bacteriochlorins…),[16] (aza)-boron-dipyrromethene ((aza)-BODIPY)[17] or (benzo)phenazine families[18] of compounds are identified as effective and known photosensitizers for such process.

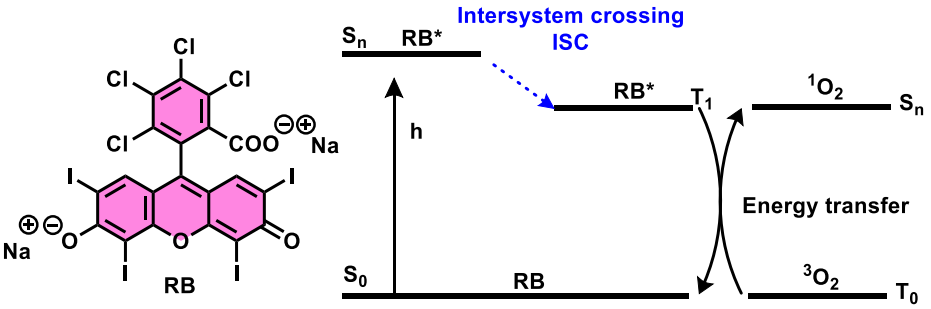

Scheme 1. Schematic representation of $^1O_2$ photoproduction using Rose Bengal as photocatalyst according to a type II mechanism.

Although organic dyes demonstrate a great potential to photogenerate singlet oxygen, these photocatalysts suffer mainly from a low photostability due to photobleaching that may be fast, a tendency to agglomerate that leads to self-quenching and a difficult elimination or recuperation at the end of a reaction.[19] It was shown that immobilizing such photocatalysts onto a solid support allows to circumvent or decrease these drawbacks while maintaining high $^1O_2$ generation efficiency.[19a, 20] Additionally, the use of heterogenized PS facilitates the recovery and reuse which has clear positive environmental and economic impacts. Additionally, an easy separation of the reaction products from the PS facilitates the work-up.[3]

Silica nanoparticles represent one of the best supports for PS immobilization since this cheap inorganic oxide possesses i) a high specific surface area that can be tuned by the porosity parameters,[21] ii) an easy-to-functionalize surface,[22] iii) transparency over a broad range of wavelengths,[23] and iv) high mechanical and (photo)stability.[21] In the generation of singlet oxygen, Rose Bengal was immobilized covalently or non-covalently onto silica nanoparticles which acted as a shield against photobleaching, thus increasing the photostability of RB and allowing its recyclability.[20a,24] Methylene

blue (MB) is another dye that has been immobilized onto silica nanoparticles leading to higher photostability in heterogeneous conditions.[20d, 25] Zinc phthalocyanines suffer from severe aggregation in aqueous medium thereby losing their singlet oxygen generation efficiency. By loading them into the modified mesopores of silica nanoparticles, phthalocyanines could generate singlet oxygen efficiently.[26] This immobilization strategy to increase the potential of organic dyes has been successfully reported in the literature for many other photosensitizers concerning singlet oxygen production[3, 19a, 27] used in organic synthesis[20b, 20d, 24a, 24b] or in medicinal applications[20f, 28].

Nevertheless, the strong immobilization of an organic dye via a covalent linker is not trivial to achieve as it usually requires its derivatization which may alter its photophysical properties and thus its photoreactivity. The impact of a molecular photosensitizer's functionalization on its photophysical properties to optimize its immobilized properties has not been investigated thus far. By displaying various positions prone to simple functionalization, (benzo)phenazines are an interesting motif to consider for such structure-activity correlations.[29] Previous investigations have focused on (benzo)phenazines in homogeneous phase to determine the best candidate for $^1O_2$ generation. Ohira, Imato and coworkers developed several phenazine derivatives to increase their $^1O_2$ generation efficiency.[18b, 18c, 18e] Surprisingly, such simple photosensitizers have not yet been investigated for $^1O_2$ generation for organic synthesis applications. So far, biological applications, such as photodynamic therapy, have been mainly targeted as highlighted by the **OR141** photocatalyst which was developed in our laboratory (**Scheme 2**).[6f, 18a, 30]

In this work, we have synthesized a series of benzo[*a*]phenazines for the production of $^1O_2$ and their use in organic synthesis, ultimately in a heterogeneous phase. Akin to a molecular compass, our methodology focused on the functionalization of three key fragments of the molecular backbone: the northern, the southern and the western fragments (**Scheme 2**). We first computationally investigated the structure-activity relationship (SAR) of the benzo[*a*]phenazines by introducing relevant moieties (electron-withdrawing or attracting groups) at different positions and identified which fragment influences the fundamental and excited-state properties the most. This is of paramount importance for the optimal immobilization of these photosensitizers. The $^1O_2$ photosensitization efficiency was evaluated using a standardized citronellol photooxidation reaction. Afterwards, the most promising candidate was anchored onto silica nanoparticles through the fragment identified as the least impactful to the ground and excited-state properties. The immobilized PS was then evaluated using the same citronellol photooxidation reaction while also assessing the recyclability.

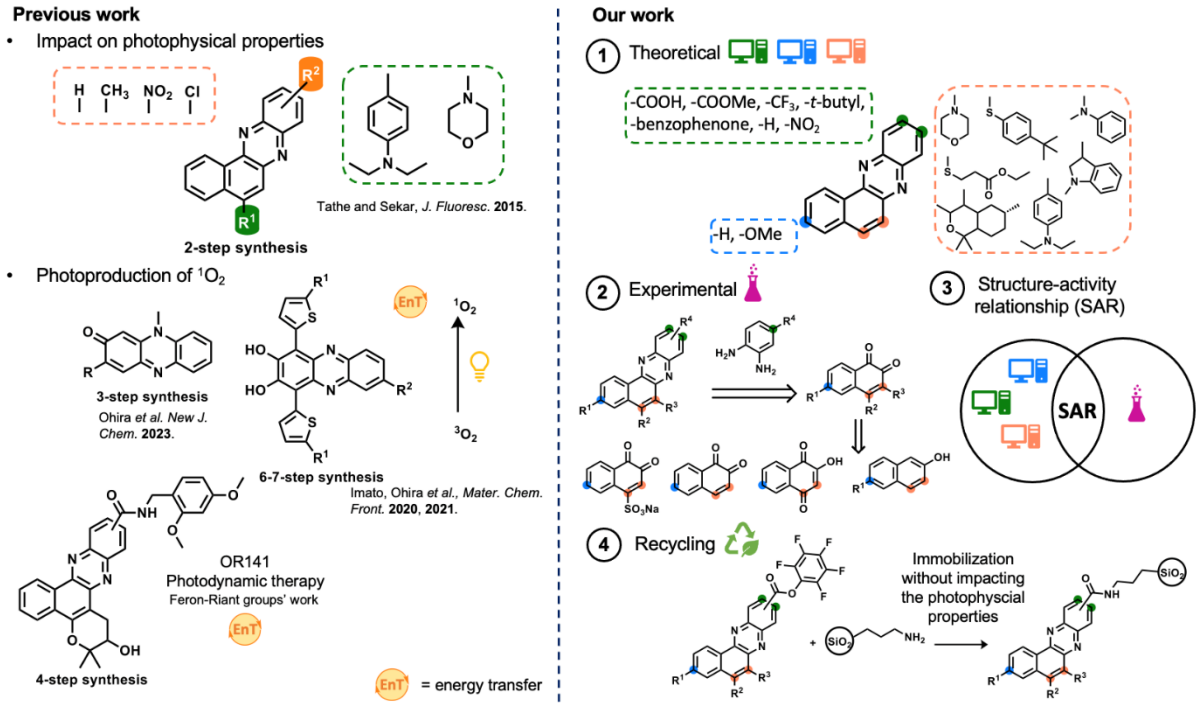

Scheme 2. State of the art of (benzo)phenazine derivatizations for singlet oxygen applications and strategy of this work.

2. RESULTS AND DISCUSSION

2.1. Cyclic ether case

Based on our envisaged methodology, a first benzo[*a*]phenazine derivative (**10a**) was targeted. Such motif is already known and investigated for biological applications as stated in recent publications[31] making its synthesis optimized and straightforward in a few steps.[29d] The first step consisted in the reaction between lawsone and *R*-citronellal generating the corresponding pyrane moiety on the southern fragment of the benzophenazine. From this reaction, a 1,2-benzoquinone (product of interest) and a 1,4-benzoquinone were produced in a 1:1 ratio, which were separated by silica gel chromatography (see SI).[31a] The second and final step consisted in condensing the synthesized methyl 3,4-diaminobenzoate with the 1,2-benzoquinone to form the benzophenazine structure and insert an ester function on the northern fragment of the molecular skeleton (**Scheme 3**).[32] The first benzophenazine structure was considered equivalent to the efficient **OR141** photosensitizer.[18a, 30a-c]

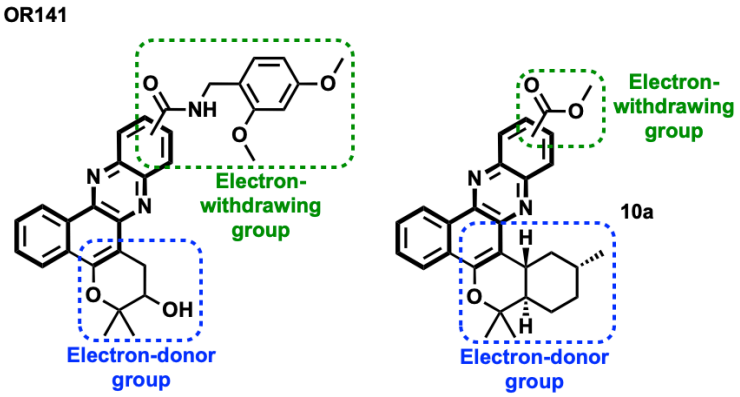

Scheme 3. Structures of **OR141** and compound **10a** presenting a benzo[*a*]phenazine core.

The photophysical properties of this new chromophore were investigated by UV-vis spectroscopy and steady-state photoluminescence. An absorption in the blue region of the visible light spectrum (427 nm, ε = 7840 M^{-1} cm^{-1}) and an emission at around 516 nm were observed (**Figure 1**).

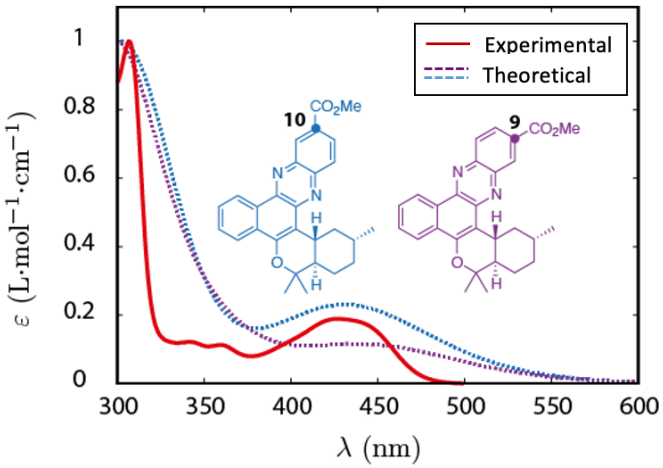

Figure 1. Comparison between the experimental (both regioisomers together) and the theoretical UV-visible absorption spectra of regioisomers of compound **10a**: influence of the position of the –CO_2Me functional group on the first monoelectronic excitation $S_0 \rightarrow S_1$.

It should be noted that during the condensation step, two regioisomers were produced, as positions 9 and 10 of the benzophenazine structure can hold the carboxylate group (identified by * in the following schemes). These regioisomers are inseparable in most cases. However, this is not a problem as the absorption and emission properties are expected to be similar. Tathe and Sekar, who synthesized benzophenazines using the same methodology as the one used in this work, did not separate the isomers and the photophysical properties were investigated with both regioisomers.[32] Furthermore, the first monoelectronic excitations $S_0 \rightarrow S_n$ (n = 100) have been calculated via time-dependent DFT with the hybrid generalized gradient approximation functional mPWPW91 recommended for organic molecules[33] and selected *via* a benchmark (see SI for details). The triple-ζ Alhrichs basis set Def2-TZVP[34] has been employed with implicit solvation (solvation model based on density (SMD), in acetonitrile ($\epsilon = 35.688\ \mathrm{F \cdot m^{-1}}$)) with the use of Gaussian 16 RevB.01.[35] The theoretical UV-visible spectrum of compound **10a** with the two possible positions of the CO_2Me group compared to the

experimental one is represented in **Figure 1**. Interestingly, the position of this functional group has a marginal effect on the theoretical absorption value associated to the monoelectronic excitation $S_0 \rightarrow S_1$ with a slight difference of 0.05 eV between the two. The only notable difference is the absorption intensity at 427 nm that is multiplied by 1.73 when the –CO_2Me is placed on position 10.

This result then leads to considering only one of these positions, *i.e.* position 10, in the following computational study. A slight difference of 0.06 eV between experience and theory has been detected for the lowest singlet excited-state excitation, with an absorption centered around 427 nm and 431 nm for experience and theory, respectively. The nature of the first excited state of compound **10a** has been determined to be of local excitation type *via* the calculation of the charge transfer length D_{index} for which the value corresponds to 2.04 Å and the τ_{index} being negative (see SI for details).[36] The former is characterized by a monoelectronic transfer from HOMO to LUMO of mainly $\pi \rightarrow \pi^*$ nature as depicted by a canonical molecular orbitals analysis performed with the NBO 7.0 software.[37] This analysis has revealed a contribution of 37 % from the π(C(12)—C(13)) bond composing the HOMO and a 38 % contribution of the π^*(C(11)—N(15)) and π^*(C(14)—N(16)) natural bond orbitals (NBOs) constituting the LUMO, as shown in **Figure 2**. To be even more precise on the location of the orbitals involved in the electronic transitions, the localization of the electron and holes density would have been also interesting to determine computationally but this is beyond the scope of the present study.

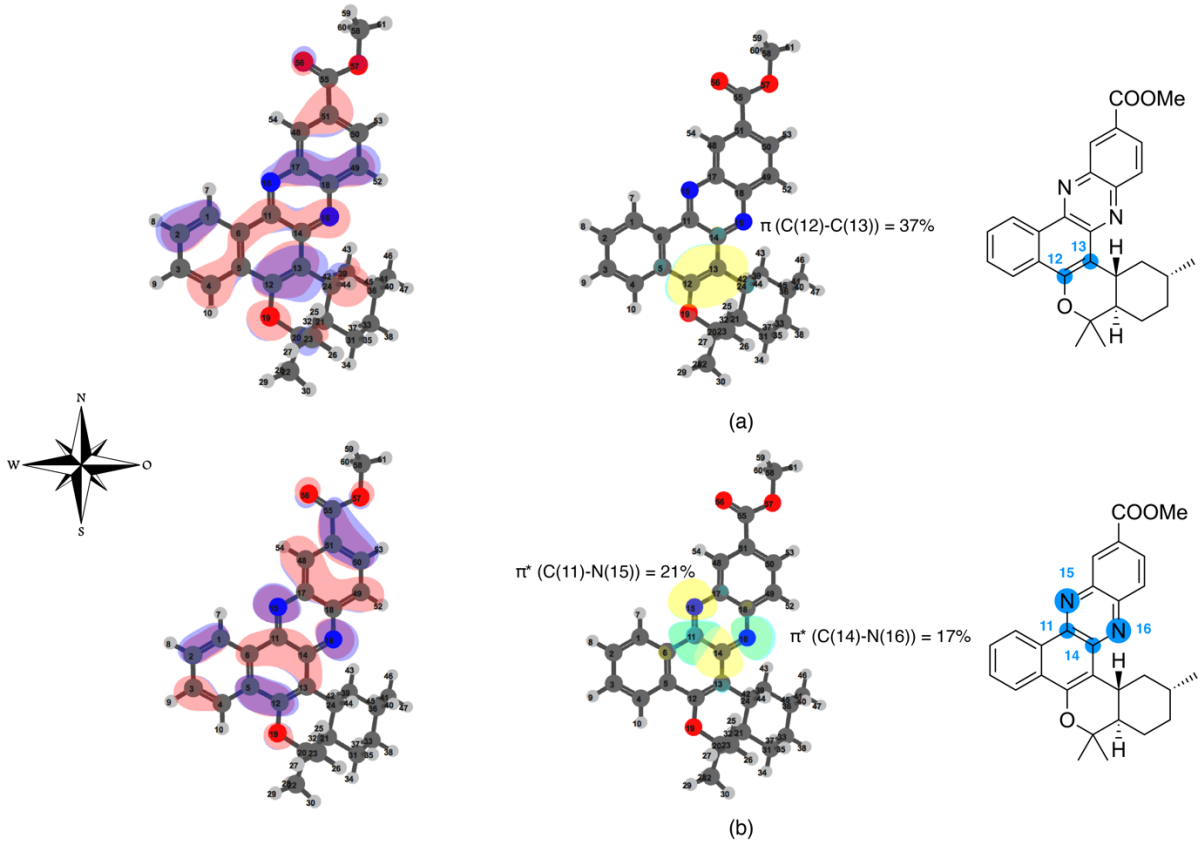

Figure 2. HOMO (a) and LUMO (b) orbitals of compound **10a** are represented on the left with positive (red) and negative (blue) orbitals along with their decomposition in their principal natural bond orbitals (NBOs) on the right.

To evaluate the ability of this dye to produce singlet oxygen, the photooxidation of citronellol was used as a benchmark reaction (**Scheme 4**). Performing this reaction in the presence of compound **10a** afforded the corresponding diols **2** and **3** (in a 1:1 ratio) with an 85 % NMR yield, identifying compound **10a** as an efficient producer of singlet oxygen.

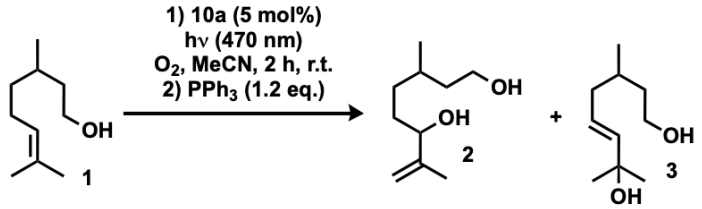

Scheme 4. Photooxidation of citronellol, used as a benchmark reaction for assessing the photoactivity of the synthesized photosensitizers.

The triplet energy of compound **10a** has been evaluated via the *Δ*SCF consisting in taking the energy difference between the geometry of the optimized ground state and the optimized triplet state in acetonitrile. A value of $40.6\ \text{kcal} \cdot \text{mol}^{-1}$ at 25 °C was determined, justifying the observed successful triplet-triplet annihilation with $^3O_2$ whose first singlet excited-state energy ($^1\Delta_g$) was experimentally measured at $22.5\ \text{kcal} \cdot \text{mol}^{-1}$ above its triplet ground state ($^3\Sigma_g^-$).[3] The Dexter energy transfer between the photosensitizer and $^3O_2$ is thermodynamically guided by the triplet energy of the chromophore. This last value can therefore be predicted prior to the synthesis of the envisioned benzophenazine derivatives. Indeed, the benzophenazine core is highly functionalizable in positions that can have an influence on the energy of the orbitals involved in the $S_0 \rightarrow S_1$ transition. Thus, the absorption wavelength will vary when the northern, southern and western fragments of the benzophenazine are modified (**Figure 2**), which is where the frontier orbitals are mainly located.

2.2. Computational prediction of the absorption wavelengths and the triplet energy of various benzophenazine derivatives

A list of synthetically accessible benzophenazine derivatives was considered for the establishment of a SAR. Such SAR could highlight the kind of moieties needed to optimize the required properties of a photosensitizer, *i.e.* the ability to absorb a low-energy photon while still having a high triplet energy excited state (**Scheme 5**). Therefore, different functionalizations addressing the areas of interest of the benzophenazine core have been considered, starting with the southern fragment.

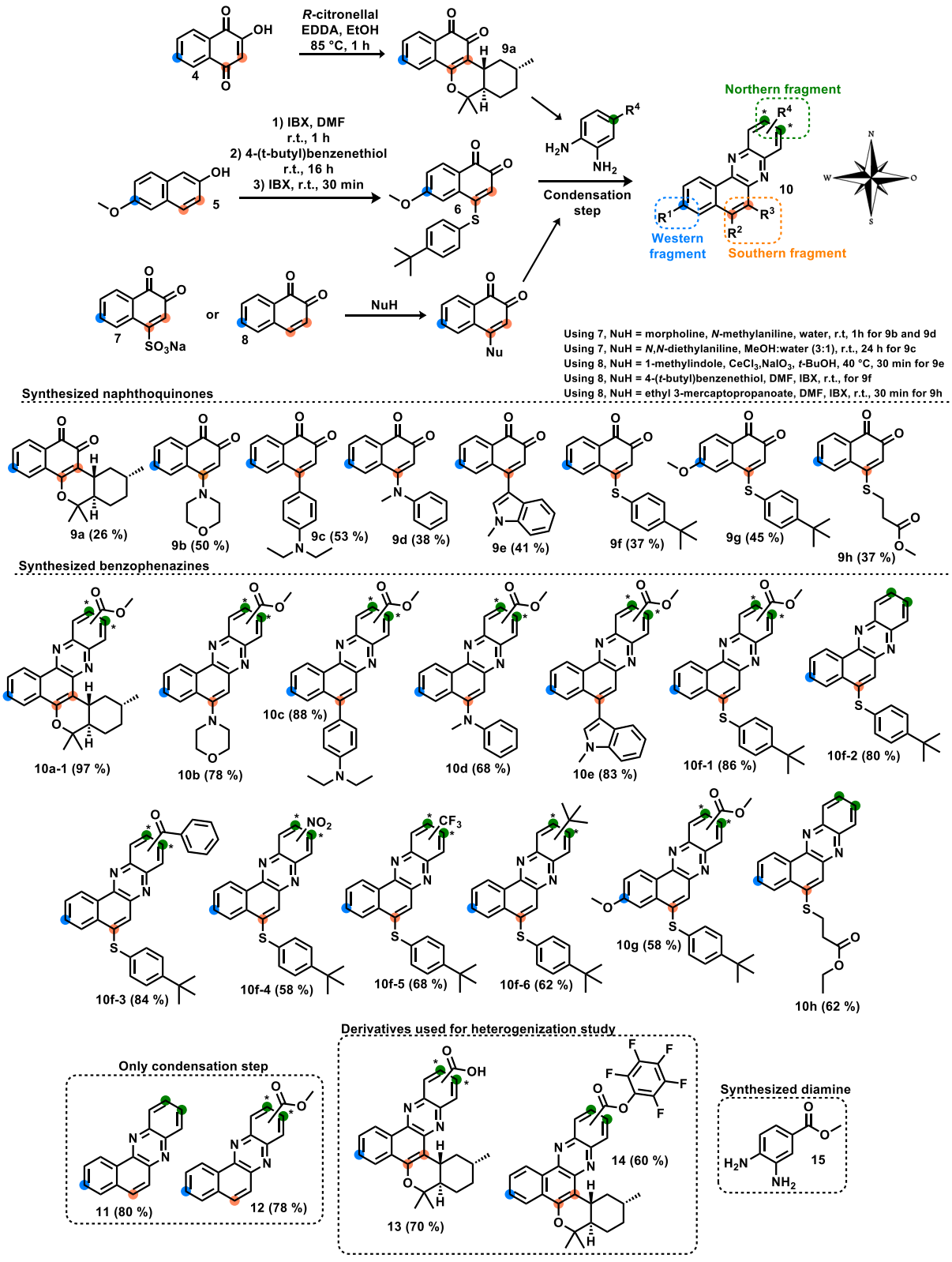

Scheme 5. Naphthoquinone and benzophenazine structures computationally investigated and synthesized in this work.

In comparison with the non-functionalized compound **12** (**Scheme 5**), the considered modifications trigger a bathochromic shift of the absorption wavelength associated with the $S_0 \rightarrow S_1$ transition (**Table 1**). This effect is particularly enhanced when using highly conjugated moieties as in

the cases of compounds **10c** and **10e**, for which an absorption in the green region of the visible spectrum is predicted. The HOMO being mainly constituted of the π C–C bond on which the functionalization is carried out, the extension of the conjugation causes the decrease of the HOMO-LUMO gap resulting in a less energetic $S_0 \rightarrow S_1$ transition. However, the nature of the excitation has been identified to be a charge transfer type for molecules **10c**, **10d** and **10e** unlike for compound **10a**, suggesting a different behavior of these derivatives in the excited state (**Table 1**). The functionalization on the southern fragment of the benzophenazine core also leads to a stabilization of the excited triplet state. It is noteworthy that this impact is relatively smaller in the case of photosensitizer **10b** and that all the derivatives are still predicted to thermodynamically favor the triplet energy transfer with $^3O_2$ in light of this computed property.

Table 1. Influence of the functionalization of the benzophenazine core on the absorption wavelength associated to the $S_0 \rightarrow S_1$ transition, the triplet energy and the nature of the monoelectronic excitation (level of theory: DFT(mPWPW91/Def2-TZVP) in acetonitrile).

Functionalized benzophenazines	**Computed absorption wavelength (nm)**	**Triplet energy (kcal · mol^{-1})**	**$S_0 \rightarrow S_1$ transition type**
12–10b–10f-1–10f-2–10f-3–10f-4–10f-5–10f-6–10g–10h	394–479–427–413–431–449–419–415–421–414	43.9–34.2–40.7–41.5–40.0–38.8–41.5–41.0–40.8–41.1	Local excitation, HOMO to LUMO ($\pi \rightarrow \pi^*$)
10c–10d–10e	567–464–502	33.6–36.7–36.2	Charge transfer, HOMO to LUMO ($\pi \rightarrow \pi^*$)

Consequently, the derivatives presenting amine functions on the southern part of the benzophenazine, except compound **10b**, are likely to be unsuitable for the photooxidation reaction due to the nature of the excitation, even though their absorption wavelength and their triplet energy are favorable for this kind of reaction. Derivative **12**, despite its important triplet energy, is also not appropriate for $^3O_2$ photosensitization because of its near UV absorption.

Going on deeper in the establishment of the SAR, the functionalization on the northern fragment of the benzophenazine was then considered with **10f-2**, the derivative displaying the highest triplet energy, an absorption in the blue region of the visible spectrum and an identical nature of local excitation when compared with compound **10a**. As opposed to the functionalization on the southern fragment of the benzophenazine, the northern one had a minor effect on the computed parameters. Indeed, compared to **10f-2**, the maximum absorption wavelength was red-shifted with electron-withdrawing groups with a maximum variation of 36 nm for compound **10f-4**, while it was nearly unchanged with an electron-donating *t*-butyl group for compound **10f-6**. The triplet energies, always remaining above 38 kcal mol^{-1}, were only slightly impacted after modifications, as presented in **Table 1**. This result is in accordance with what has been observed for the frontier orbitals of derivative **10a** in **Figure 2**. While the HOMO is mostly located where the southern functionalization is situated the LUMO is not principally located in the region of the northern functionalization. Hence, northern functionalization only leads to marginal

changes in the photophysical properties and encourages the use of $–CO_2Me$ group on the northern fragment for subsequent surface anchoring.

The western fragment of **10f-1** has also been explored via the benzophenazine **10g** (**Scheme 5**) with no strong incidence on the absorption wavelength and the triplet energy. In parallel, another sulfur-containing compound **10h**, bearing an aliphatic sulfur with an ester group, was studied for potential further modification or grafting and revealed in the same manner, no improvements of the absorption wavelength and the triplet energy.

In order to validate the computational studies, we conducted the synthesis of the different chromophores, using the same two-step procedure as described above. At first, we tackled the southern fragment variations of the benzophenazine core in order to introduce various substitutions with heteroatoms (O,N,S: **9a, 9b, 9d, 9f-h**) and carbon-based electron conjugated systems with electron–donating atoms (N: **9c and 9e**) (**Scheme 5**), using adapted reported procedures from the literature.[29c, 29d, 31a, 38] In most cases, a Michael addition with an heteroatom or carbon-based nucleophile on the corresponding naphthoquinone **8**, or its sulfonate adduct **7**, allowed to access the desired 1,2-naphthoquinone in a single step. For the 6-methoxy-derivative **9g**, the starting 2-naphthoquinone **6** was generated *in situ* by IBX (2-iodoxybenzoic acid) oxidation of the corresponding 6-methoxynaphthalen-2-ol **5**.[29d] Finally, naphthoquinone **9a** was easily prepared by condensation of hydroxynaphthoquinone **4** with *R*-citronellal *via* well-known reported procedures.[31a] These photosensitizers were obtained in the range of 21 and 47 % yields over two steps.

2.3. Experimental photophysical properties

In order to establish a structure-activity relationship, references are needed to evaluate the impact of the functionalization on one of the key fragments of the molecular skeleton of benzophenazines. For the southern fragment, compound **12** was used to evaluate the impact on the fundamental and excited states, compound **10f-1** for the influence on the generation of singlet oxygen, and compound **10f-2** was only used as a reference for the compound **10h** to assess the impact of the presence of aromatic or aliphatic sulfur. For the northern fragment, compound **10f-2** was the reference and for the western fragment, compound **10f-1** served as reference (**Scheme 6**).

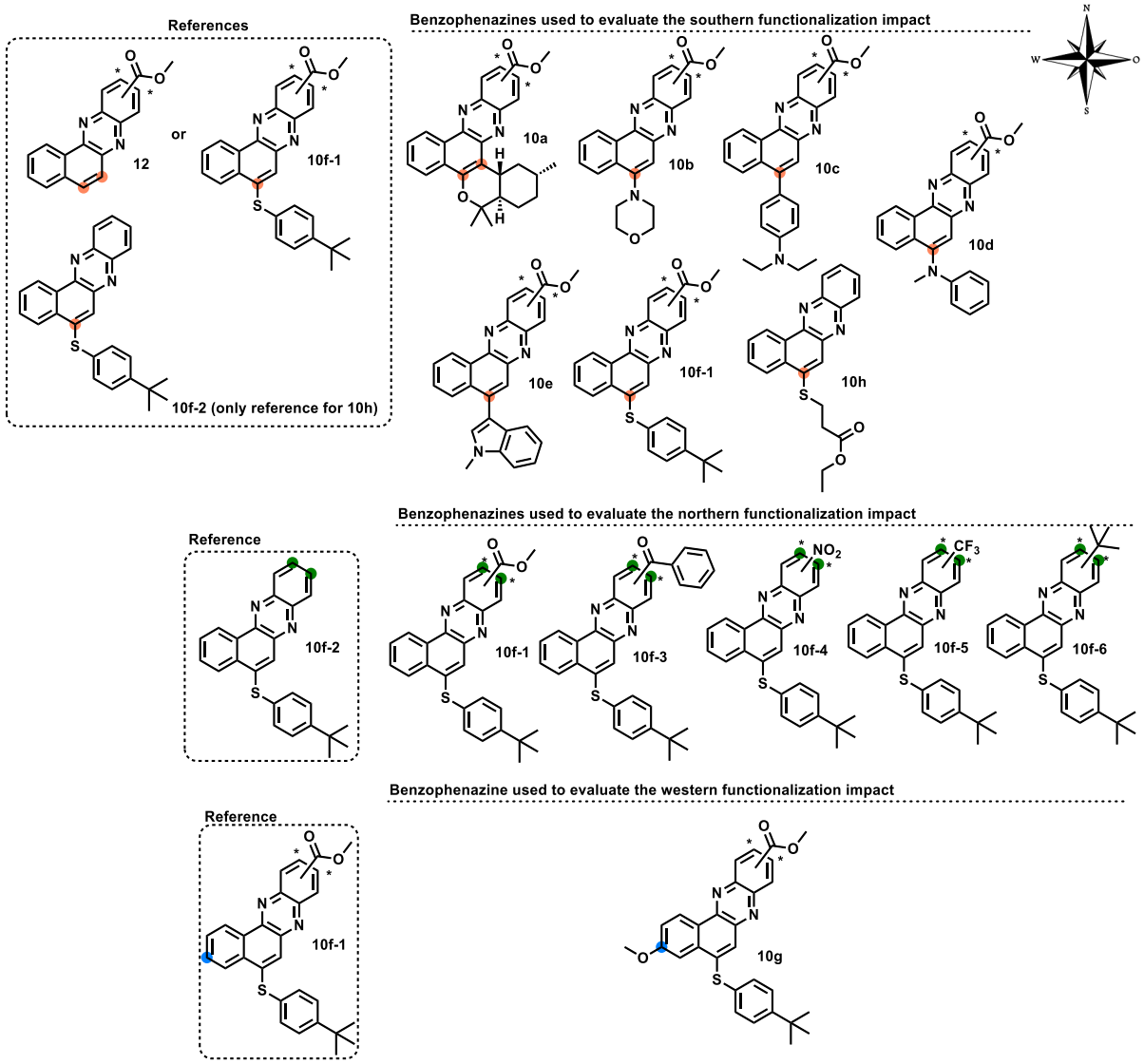

Scheme 6. References used to evaluate the impact of functionalization on key fragments of benzophenazines.

The impact of functionalization on the UV-Visible absorption properties were first investigated in acetonitrile (**Table 2**). Compound **12** absorbed mostly in the UV range and had a contribution in the visible range with a maximum centered at 408 nm (molar absorption coefficient ε of 13,200 M^{-1} cm^{-1}) that tailed until 435 nm. The considered functionalizations on the southern fragment led to a bathochromic shift in the absorption wavelengths which was more important for compounds **10c**, **10d** and **10e**, as expected for compounds **10c** and **10e** based on the computational results. While enhancing the ability to absorb in the visible range, the functionalization on the southern fragment generally decreased the molar extinction coefficient which was particularly striking for compounds **10d**, **10e** and **10a** (below 10,000 M^{-1} cm^{-1}). Compound **10h** on the other hand, was marginally affected (when compared to compound **10f-2**). The northern fragment had a moderate impact on the photophysical properties of the benzophenazines with a peak maximum variation of 15 nm for **10f-4**. The introduction of the slightly electron-donating *t*-butyl group had no impact at all on absorption properties whereas electron-withdrawing groups tended to give bathochromic shifts. For molar absorption coefficients, the

impact of functionalization was stronger and of considerable importance for the NO_2 moiety for which it was divided by more than half. This result is quite surprising as the CF_3 motif did not give such a decrease of ε. The western fragment derivatization also had a detrimental effect on the molar absorption coefficient while the absorption wavelength was unchanged (**Figure 3**). Based on these findings, it can be concluded that all functionalizations led to a decrease of the molar absorption coefficient while the absorption wavelength was most impacted through the southern fragment. The latter was expected since the computational studies identified the location of the HOMO on that part of the molecule.

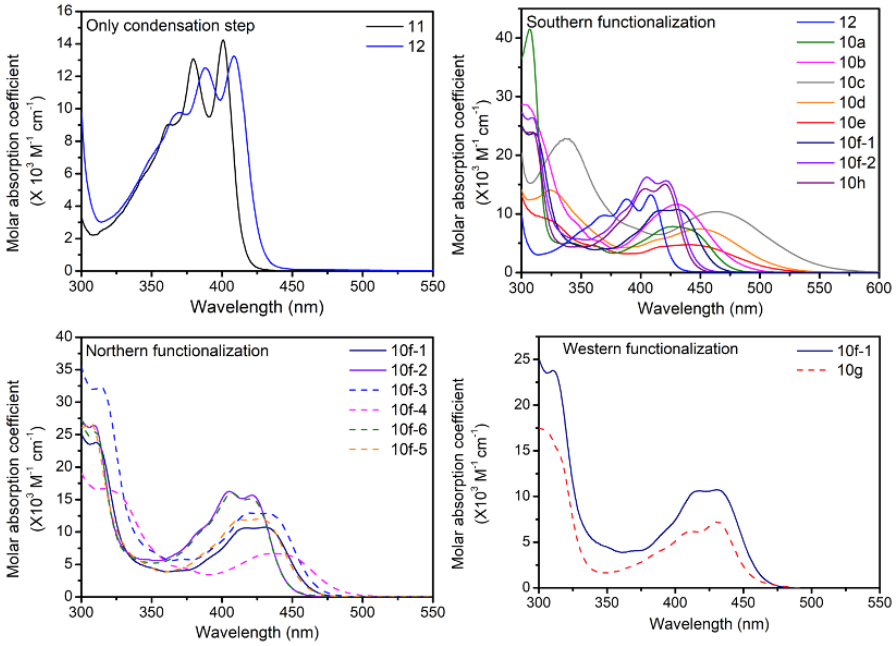

Figure 3. UV-vis absorption spectra of benzophenazine derivatives, recorded at room temperature in acetonitrile.

Visible light excitation of benzophenazine derivatives led to steady-state photoluminescence (SSPL) centered between 469 and 609 nm for fluorescence signals (**Figure S2**). Similarly to the UV-vis absorption measurements, a red-shifted emission was observed for benzophenazine derivatives functionalized on their southern fragment. The presence of oxygen and nitrogen heteroatoms and carbon-based electron conjugated systems with nitrogen atoms on that fragment exhibited a blue-shifted fluorescence signal compared to compound **12**. The sulfur-based derivatives, on the other hand, showed higher energetic singlet excited states. When comparing compounds **10f-2** and **10h**, the aromatic sulfur seems to stabilize the singlet excited state more than the aliphatic sulfur as their fluorescence peaks are centered at 529 and 477 nm, respectively. The modifications on the northern fragment, irrespective of the presence of an electron-donating or -withdrawing group, provoked an emission blue-shifted by ~40 nm. As for the western fragment, it only had a slight influence on emission properties (emission red-shifted by 10 nm for **10g**).

To further characterize this singlet excited state, time-resolved photoluminescence (TRPL) measurements in acetonitrile were conducted to determine the fluorescence lifetime. The experimental

data points were well described by first-order kinetics which yielded short excited singlet state lifetimes of around 5 ns. For the sulfur-based derivatives, the fluorescence lifetime could not be measured as it was below the instrument response. These short excited singlet state lifetimes can be due to a fast intersystem crossing (ISC) leading to a triplet state from which a phosphorescence signal can be emitted. If an ISC quantum yield of 1 would be effective, no fluorescence at all would have been observed. This phenomenon would explain the short excited singlet state lifetime of sulfur-based compounds as the sulfur atom favors the spin-orbit coupling, and thus populates its excited triplet state from which a phosphorescence signal can be observed.[39]

To investigate this excited triplet state, *i.e.* the phosphorescence signal, the photoluminescence intensity was measured 100 ns after a laser pulse. An emission signal was indeed detected and could be attributed to a phosphorescence signal which ranged from 482 to 609 nm (**Figure S3**). The southern fragment had no influence on the phosphorescence signal. On the northern fragment, however, the electron-withdrawing groups caused a red-shifted emission while the *t*-butyl group caused a blue-shifted one, highlighting that electron-donating groups could lead to an increased excited triplet state energy. The –OMe functionalization on the western fragment displayed also a quite important blue-shifted phosphorescence emission compared to compound **10f-1**. These maxima values of emission can be used to approximate the experimental triplet energy value, even if this methodology underestimates the triplet energy. With the emission wavelength ranging from 482 to 609 nm, all compounds have a high triplet energy that is enough to photosensitize $^3O_2$, as predicted by the computational study. Based on the scale of energy (**Table 2** and **Figure S5**), photosensitizers **10e**, **10h** and **10g** were identified as the best compounds to photosensitize oxygen. Surprisingly, for compounds **10d** and **10e**, the triplet state was higher in energy than the singlet state, leading to a positive singlet-triplet energy gap. This inverted energy gap is mainly investigated for organic light-emitting diodes (OLED) to increase the quantum efficiency.[40] This positive gap is peculiar as for the vast majority of molecular systems, T_1 state lies energetically below the S_1 state due to exchange interactions which stabilize triplets and destabilize singlets.[40a] When the HOMO and the LUMO are spatially nonoverlapping, these exchange interactions can become very small and can lead to inverted gaps. This applies, in particular, for internal charge-transfer excitation that minimizes the exchange interactions.[40c] Based on our computational results, methylaniline **10d** and indole **10e** derivatives possess a S_0 to S_1 internal charge transfer and this would explain this anomaly. As an inverted gap is highly difficult to obtain experimentally, another hypothesis needs to be considered. Indeed, the time-delayed emission spectra are not of high quality (very broadened) and could suggest that different electronic transitions, such as $\pi - \pi^*$and an internal charge transfer from the donor nitrogen, proceed under irradiation leading to different excited states with different energies. Such combinations of excited states could potentially explain this anomaly. Computations could intervene to determine the excited-state energies of both electronic transitions in order to validate or not our hypothesis. This hypothesis of a mixture of excited states can be reinforced

when taking a look at the phosphorescence emission of north-ester and south-aromatic sulfur **10f-1** and west-OMe **10g** which differ by 75 nm. That difference is too important to be only due to the introduction of a methoxy group on the western fragment of the benzophenazine and could be explained by the presence of a mixture of excited states.

Having a high triplet excited-state energy is important to photosensitize oxygen but it is not the only pre-requisite as the photosensitizer also needs a long excited triplet state lifetime to perform energy transfers. Hence, triplet excited-state lifetimes were measured 100 ns after the laser pulse (again to avoid any fluorescence contribution) by integrating the signal at different time intervals (**Figure S4**). The measured lifetimes were around a few microseconds in most cases, with the lowest values exhibited by compounds **10c**, **10d** and **10e**. These lifetimes are long enough to allow energy or electron transfers (**Table 2**). The functionalization on the southern fragment was valuable for the triplet excited-state lifetime. Indeed, the presence of heavy atoms, such as sulfur which are known to enhance the ISC quantum yield, led to a phosphorescence lifetime of 4.5 μs for compound **10f-1** while it dropped below 2 μs when nitrogen moieties were present.[41] Thus, indole **10e**, methylaniline **10d** and diethylaniline **10c** derivatives are probably less efficient photosensitizers. Moreover, the computational study revealed the different nature of their excited states which reinforces these statements. The use of an aliphatic sulfur as a southern fragment (**10h**) enhanced the phosphorescence lifetime of the molecule, bringing it to nearly double the value of its reference **10f-2**. Interesting triplet excited-state lifetimes were also reached with derivatives **10b** and **10a**, even though no heavy atom was introduced. The derivatization of the northern fragment of molecular skeleton had a positive impact on the triplet excited-state lifetimes as the presence of electron-withdrawing or -donating groups increased these values from 2.2 μs for the reference **10f-2** to a maximum value of 5.4 μs for compound **10f-4** with a NO_2 motif, which is the longest triplet lifetime of all the benzophenazines synthesized in this work. The introduction of a methoxy group on the western fragment (**10g**) negatively impacted the phosphorescence lifetime since the value dropped to 3.0 μs compared to 4.5 μs for the reference **10f-1**.

Table 2. Photophysical properties of benzophenazine derivatives. Steady-state and time-resolved photoluminescence spectra were recorded in argon-purged acetonitrile. Phosphorescence signals were recorded 100 ns after the laser pulse at different time intervals. IRF = Instrument Response Function

	Absorption (nm)	**ε ($M^{-1}cm^{-1}$)**	**Fluo./ Phospho. (nm)**	**Fluo. lifetime (ns)**	**Phospho. lifetime (μs)**	**Triplet state energy (kcal/mol)**
Southern fragment functionalization						
Reference 12	408	13.200	469/561	n.d.	n.d.	50.9
Reference 10f-2	421	15.600	529/539	< IRF	2.2	53.0
10a	427	7840	516/516	2.6	3.0	**55.4**
10b	431	11.650	609/609	6.9	**4.6**	46.9
10c	**463**	10.380	500/564	5.1	0.3	50.7
10d	**449**	7450	569/538	5.3	0.8	53.1
10e	440	4760	530/482	4.7	1.1	**59.3**
10f-1	431	10.730	476/569	< IRF	**4.5**	50.2
10h	420	15.060	477/477	< IRF	**3.9**	**59.9**
Northern fragment functionalization						
Reference 10f-2	421	15.600	529/539	< IRF	2.2	53.0
10f-1	431	10.730	476/569	< IRF	**4.5**	50.2
10f-3	432	12.870	475/572	< IRF	2.6	50.0
10f-4	436	6660	481/549	< IRF	5.4	52.1
10f-5	427	12.050	476/578	< IRF	2.6	49.5
10f-6	421	15.110	483/522	< IRF	3.0	**54.8**
Western fragment functionalization						
Reference 10f-1	431	10.730	476/569	< IRF	4.5	50.2
10g	431	7240	486/494	< IRF	3.0	**57.9**

Although having a long triplet excited-state lifetime could increase the efficiency of a photosensitizer, the triplet state also needs to be highly populated to ensure strong O_2 photosensitization. An ISC quantum yield close to the unity leads to an efficient and fast access to a triplet state that is highly populated by excited molecules and is translated by an intense phosphorescence intensity. **Figure 4** shows that all sulfur benzophenazine derivatives exhibited the strongest photoluminescence intensity which was expected since heavy atoms increase the spin-orbit coupling.[42] The ISC quantum yield also depends on the energy gap existing between S_1 and T_1 (ΔE_{ST}). Small ΔE_{ST} values are more conducive to increase the ISC quantum yield.[41] This dependency is observed with compound **10h** exhibiting the most important intensity of phosphorescence among all of the sulfur-based PS with the smallest ΔE_{ST}. An

exception was observed for compounds **10f-4** and **10g** for which the presence of a NO_2 moiety on the northern fragment and the presence of a methoxy group on the western one were detrimental, respectively, and lowered the efficiency of the ISC conversion. Despite having the longest phosphorescence lifetime, the photoactivity of the NO_2 benzophenazine derivative **10f-4** could be low as the triplet state is not occupied enough leading to only a small fraction of excited molecules capable of transferring energy to triplet oxygen. This peculiar behavior is interesting since average photophysical properties were obtained with the CF_3 moiety (**10f-5**), which is also an efficient electron-withdrawing group, confirming again the specific impact of a NO_2 moiety on the photophysical properties. Photosensitizer **10a** is promising as it exhibited the second most intense photoluminescence with an average triplet lifetime. Although no heavy atom is present, the ΔE_{ST} is small and could explain this observed high ISC quantum yield. On the contrary, benzophenazines with a nitrogen moiety on the southern fragment showed poor results and reinforce the hypothesis of being non-suitable triplet oxygen photosensitizers.

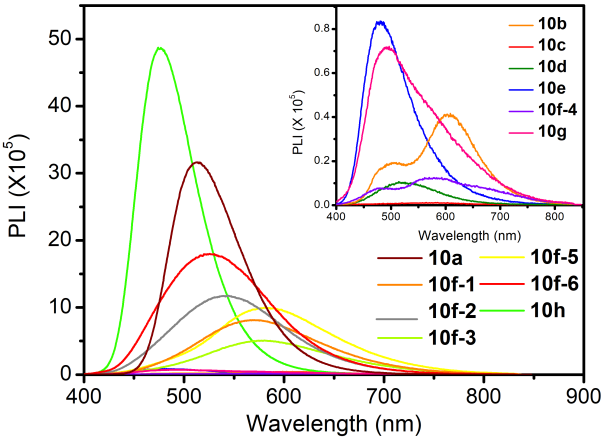

Figure 4. Photoluminescence intensity spectra of benzophenazine derivatives. Inset: zoom in case of low PLI.

2.4. $^3O_2$ photosensitization

It is known that the photosensitization of oxygen leads to the production of reactive oxygen species, such as $O_2^{\bullet-}$, hydroxyl radical, H_2O_2, singlet oxygen…[41, 43] The excited-state quenching of benzophenazine derivatives was highlighted by their decreased photoluminescence intensity in presence of oxygen (**Figure S6**). In order to evaluate the selective production of singlet oxygen, quantum yields (ϕ_Δ) for $^1O_2$ generation by benzophenazine derivatives were evaluated by monitoring the changes in absorption of anthracene-9,10-divinylsulfonate (AVS), anthracene-based fluorescence probes being known as selective for singlet oxygen (**Figure S7**).[44] At regular intervals, the absorption spectra of AVS in presence of a given PS and under irradiation was measured in DMSO and the difference in absorption was plotted against time to determine the quantum yields for $^1O_2$ generation. This experiment was conducted three times for each different photosensitizer. The same trend was observed as before, the sulfur-based derivatives and compound **10a** exhibiting quantum yields varying between 0.84 and 0.59 (the highest one being attributed to the aliphatic sulfur compound **10h**) which is in the same range

as Rose Bengal, famous $^3O_2$ PS, which was used as reference ($\phi_\Delta = 0.76$ in water, **Figure S8**).[20a] The oxygen quantum yields obtained are also comparable to methylene blue ($\phi_\Delta = 0.51$), $[Ru(bpy)_3]^{2+}$ (bpy = bipyridine, $\phi_\Delta = 0.73$), tetraphenylporphyrin ($\phi_\Delta = 0.78$) or 4-phenylbenzophenone ($\phi_\Delta = 0.75$)[19a] which highlights the good performances of our new synthesized photosensitizers. On the southern fragment, the family of derivatives carrying substituents with an amine function were either poorly active: $\phi_\Delta = 0.05$ and 0.04 for indole **10e** and diethylaniline **10c** derivatives, respectively, or not active at all (compound **10d** showed a decrease in absorbance of AVS identical to the control test which consisted in irradiating AVS alone (**Figure S9**)). The singlet oxygen quantum yield for morpholine derivative **10b** could not be measured due to incompatibility in reaction conditions. The southern fragment is again identified as having a lot of influence on the reactivity of our photosensitizers. For the northern fragment, the use of electron-withdrawing groups increased the singlet oxygen quantum yield while the use of the *t*-butyl electron-donating group changed only slightly the value. An exception was made for the peculiar photosensitizer bearing a NO_2 motif whose ϕ_Δ decreased as nearly no singlet oxygen was produced ($\phi_\Delta = 0.07$), which confirmed that its behavior is different from the sulfur derivatives. The western fragment had no influence on the production of singlet oxygen.

Table 3. Investigated parameters for the $^3O_2$ photosensitization by benzophenazine derivatives.

	$^1O_2$ quantum yield[a]	Citronellol photooxidation (%)[b]
Southern fragment functionalization		
Reference 10f-1	**0.80**	**98**
Reference 10f-2	**0.59**	**98**
10a	**0.70**	**85**
10b	-	83
10c	0.04	7
10d	0	15
10e	0.05	34
10h	**0.75**	**92**
12	n.d.	96[c]
Northern fragment functionalization		
Reference 10f-2	**0.59**	**98**
10f-1	**0.80**	**98**
10f-3	**0.84**	**99**
10f-4	0.07	32
10f-5	**0.83**	**93**
10f-6	**0.64**	**98**
Western fragment functionalization		
Reference 10f-1	**0.80**	**98**
10g	**0.82**	**95**

[a] The singlet oxygen quantum yield was corrected taking into account the degradation of AVS alone under blue irradiation with blue Thorlabs lamps. [b] NMR yield determined with dimethylsulfone as internal standard. [c] Two LED IP FL-30 (eurolite) with an emission wavelength of ~390 nm were used.

Finally, all benzophenazine derivatives were evaluated in the photooxidation of citronellol, with the same reaction conditions as presented in **Scheme 4** (for which the simultaneous presence of PS and light was highlighted as necessary with control tests (**Scheme S1**)). Based on the photophysical properties and the ability to perform energy transfer with oxygen, sulfur derivatives (except for compound **10f-4**) were expected to be efficient. Indeed, a high NMR yield of desired products was obtained, ranging from 99 to 92 % (compound **10f-4** is not considered). The presence of electron-donating or -withdrawing groups on the northern fragment had no influence on the activity of the benzophenazines. The morpholine derivative **10b**, with its long phosphorescence lifetime, was performant and an NMR yield of 83 % was obtained. This compound is the only one in the family of derivatives carrying an amine function that exhibited a photocatalytic activity. Indole **10e**, methylaniline **10d** and diethylaniline **10c** derivatives were not efficient in the $^1O_2$ photooxidation of citronellol with NMR yields of 34, 15 and 7 %, respectively. Compound **10g** was as performant as the reference **10f-1**, highlighting the inertness of the western fragment for the production of singlet oxygen. The generation

of singlet oxygen was reproducible as the citronellol photooxidation was performed three times with compounds **10b**, **10a** and **10h** with an average yield of 79±7, 86±1 and 94±4 %, respectively.

2.5. Photostability investigation

The photostability of the different photosensitizers was then investigated over the course of 2 hours. The photostability of compounds **10f-1** (**Figure 6**), **10b** (**Figure S10**) and **10a** (**Figure 5**) were evaluated by monitoring their absorption and emission spectra under different reaction conditions, *i.e.* under irradiation, under irradiation in presence of oxygen and under irradiation in presence of oxygen and citronellol. A change in absorbance along with a decrease in photoluminescence intensity would be the sign of a photodegradation. Compound **10f-1** showed a very slight decrease in absorbance when it was irradiated alone meaning that no photodegradation was induced by light. The difference in absorbance was more important in presence of oxygen but decreased when citronellol was also present in the mixture. This PS is therefore slightly sensitive to singlet oxygen but can be considered photostable when another molecule that can react with singlet oxygen is present. The same trend was observed with the emission spectra. We went one step further by analyzing the filtrates with compound **10f-1** by HRMS to be sure that the structure of the PS was not altered. The characteristic peak of the PS was observed and no other peaks were found at higher *m/z* ratio, excluding the hypothesis of forming a sulfoxide or sulfone moiety onto the PS structure in presence of singlet oxygen. Compound **10b** was also photostable but the presence of citronellol did not decrease its photodegradation meaning that this PS was more sensitive than compound **10f-1** but was still highly photostable. Finally, the photostability of compound **10a** was investigated and nearly no photodegradation was observed on absorption and emission spectra under the three different conditions tested.

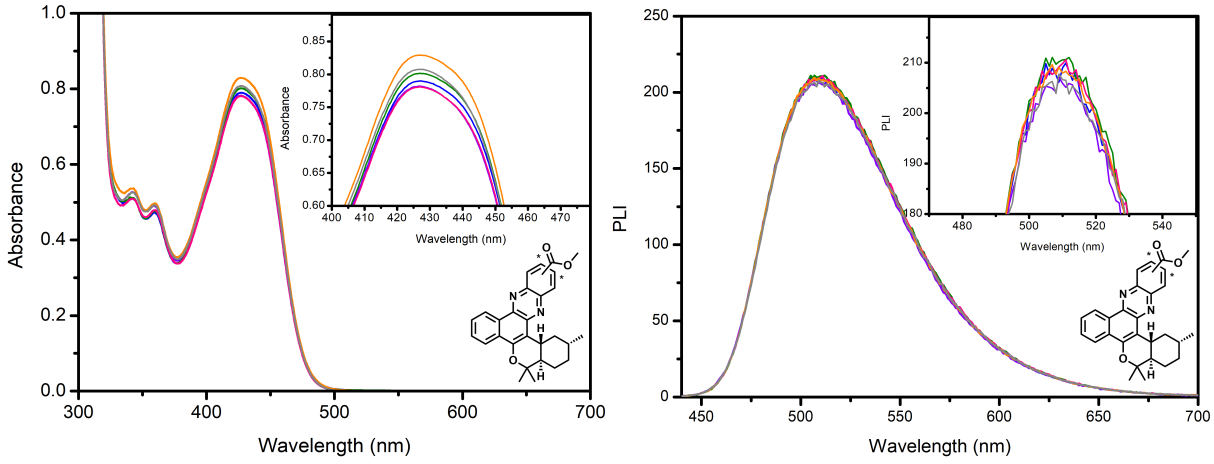

Figure 5. Absorption (left) and steady-state photoluminescence (right) spectra of photosensitizer **10a** before (blue) and after (purple) 2 hours of irradiation, before (green) and after (pink) 2 hours of irradiation in presence of oxygen, and before (orange) and after (grey) 2 hours of irradiation in presence of oxygen and citronellol. The insets correspond to a zoom in the zone of interest.

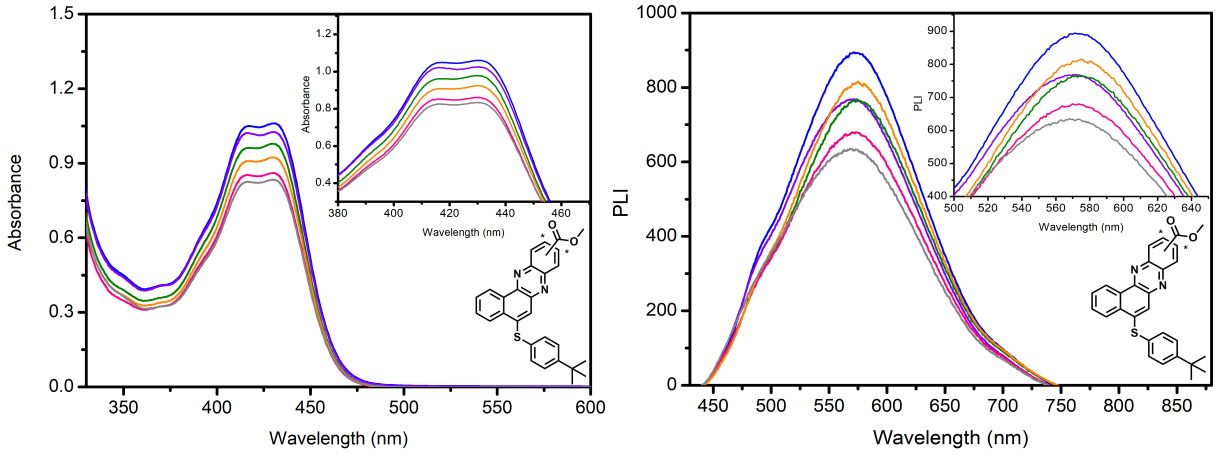

Figure 6. Absorption (left) and steady-state photoluminescence (right) spectra of photosensitizer **10f-1** before (blue) and after (purple) 2 hours of irradiation, before (green) and after (pink) 2 hours of irradiation in presence of oxygen, and before (orange) and after (grey) 2 hours of irradiation in presence of oxygen and citronellol. The insets correspond to a zoom in the zone of interest.

Note that the NO_2 **10f-4**, diethylaniline **10c**, indole **10e** and methylaniline **10d** derivatives being not efficient PS, the functionalization of compound **10g** having no strong positive impact on its photophysical properties and its photoactivity, and the functionalization of **10h** being located on the southern fragment that could alter a lot the photophysical properties, the photostability of these compounds were not assessed.

So far, the sulfur-based photocatalysts were the best to produce singlet oxygen. However, compound **10f-1** did not exhibit the highest photostability which is a crucial characteristic in heterogeneous photocatalysis. Indeed, more photodegradation was observed for compound **10f-1** compared to **10a** for each tested condition. For this reason, compound **10a** was selected for the heterogenization study as it displayed excellent efficiency in producing singlet oxygen together with high stability.

2.6. Benzophenazine heterogenization on silica nanoparticles

We have identified that the northern fragment functionalization of a benzophenazine has little impact on the photophysical properties or the photoactivity of the PS and we can then, therefore, take advantage of a carboxylic acid derivative to carry out the heterogenization of the PS on silica nanoparticles. Compound **10a** was the PS of choice to conduct this recyclability study as it exhibited excellent performances and the highest photostability of all the investigated benzophenazine derivatives. The envisaged methodology is to add an activated ester on the northern fragment of compound **10a** that could react with amino-functionalized silica nanoparticles to form a photostable covalent amide linker (**Scheme 7**).

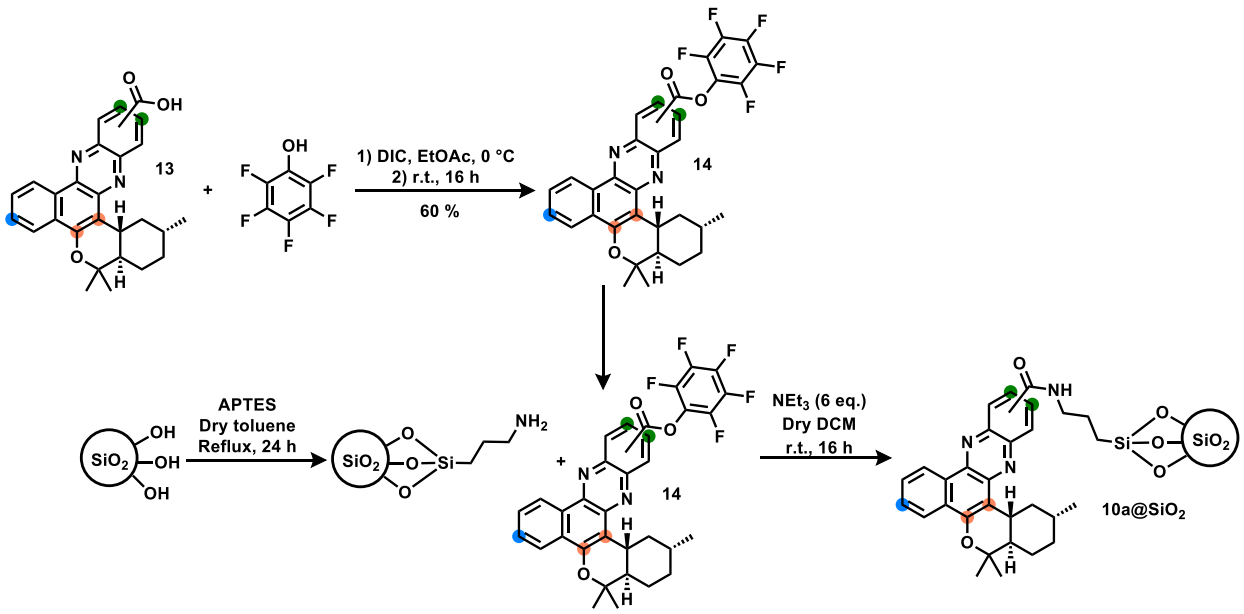

Scheme 7. Envisaged methodology for the heterogenization of photosensitizer **10a**.

The first step towards the heterogenization of compound **10a** was the synthesis of the activated ester derivative **14** that would allow the formation of covalent bonds with the modified silica surface. An acid-derivative **13** was needed which was easily obtained in the same two steps as compound **10a**, except that 3,4-diaminobenzoic acid was used instead. The acid-derivative **13** reacted with pentafluorophenol in presence of *N*,*N*'-diisopropylcarbodiimide (DIC) in ethyl acetate to afford the corresponding activated ester with a 60 % isolated yield.

With the activated ester photosensitizer **14** in hands, we sought to develop the synthesis of silica nanoparticles for efficient surface immobilization. Nanospheres (NS) were targeted as these represent a standard morphology that prevents potential pore-diffusion issues, as commonly observed in heterogeneous catalysis.[24b, 45] Nanospheres were obtained by adapting the procedure of Stöber *et al.* based on the sol-gel process to access a 40 nm diameter size.[46] The size and morphology of these NS nanoparticles were confirmed by transmission electron microscopy (TEM) (**Figure S11**) and dynamic light scattering (DLS) (**Figure S12**). Specific surface area of 360 m^2 g^{-1} was calculated using the Brunauer-Emmett-Teller (BET) equation on nitrogen physisorption data (**Figure S14**). Concerning the pores size and the porous volume, Density Functional Theory (DFT) method was used as a standard protocol for microporous materials. Nanospheres exhibit micropores of mean size 0.7 nm and a porous volume of 0.63 cm^3 g^{-1}.

In order to form the covalent bond between the support and the PS, some amino-functions were needed at the surface of NS nanoparticles. *Via* the silanol chemistry of these NS nanoparticles, aminopropyltriethoxysilane (APTES) was grafted onto the surface using inert conditions to avoid the fast and possible polymerization of this silane.[22d] The efficient grafting of amine functions was confirmed by X-Ray photoelectron spectroscopy (XPS) where a N_{1s} peak at 399.8 eV was observed, which is characteristic of amine moieties (**Figure S16**). As XPS is a semi-quantitative surface analysis,

a thermogravimetric analysis (TGA) was recorded to quantify the loading of amino groups at the surface of the support (**Figure S15**). The thermogram showed a loss in weight of about 12 wt.% which corresponds to 0.10 mmol of amino functions per 100 mg of material.

The NS nanoparticles with amine moieties immobilized at their surfaces were dispersed in dichloromethane and allowed to react with the activated ester **14** in presence of triethylamine during 16 h to afford the heterogenized photosensitizer denoted **10a@SiO$_2$**. This afforded a yellowish powder that was characterized by XPS and TGA. All expected elements were detected at correct binding energy by XPS and the atomic ratios were close to the expected ones, indicating that the organic dye's structure was intact on the surface (see page **S33** in SI, **Tables S2** and **S3** and **Figure S18**). A TGA thermogram was recorded to evaluate the quantity of grafted PS and showed a loss in weight of about 20 wt.% (**Figure S15**). By calculating the difference between the loss in weight of the amino-functionalized NS nanospheres and the one of grafted PS, we determined a 7.8 wt.% loading in PS, which corresponds to 0.02 mmol of PS per 100 mg of material.

The photocatalytic activity of **10a@SiO$_2$** was then investigated using the citronellol photooxidation benchmark reaction (**Scheme S1**). Knowing the adsorption/desorption equilibria that occurs before and after the reaction and the potential loss of singlet oxygen through interaction with the support, the time of reaction was increased to 16 h. The first run of reaction gave a very satisfying 97 % NMR yield which proved that the photophysical properties were maintained after heterogenization. A bright yellow powder was recovered at the end of the reaction which was promising for future recyclability tests. Three consecutive recycling runs were conducted and 96, 91 and 85 % NMR yields were obtained for the second, third and fourth run, respectively.

To understand the slight decrease in activity of the heterogenized PS along the runs, the final material was analyzed by XPS (**Figure 7**). Nitrogen, which is the characteristic element of our dye, was still detected at the surface with an atomic percentage (at.%) of 3 at an appropriate binding energy of 400 eV. Based on this, we could calculate an approximative leaching of 25 %, which could explain the decrease in photoactivity. This leaching is overestimated if some amine moieties that did not react with the activated ester **14** are leached which could explain the decrease of the NR_4^+ component in the N_{1s} signal after 4 runs. Another explanation for this component decrease is that primary amines can interact with silanol groups through H-bonds. Such interaction is impacted by the solvent polarity and decrease in the presence of a polar solvent. In our case, the use of polar acetonitrile could then explain the lower amount of detected quaternary amines. Moreover, the N/C ratio (0.15) was similar to the initial one (0.13), indicating that the PS may have conserved its molecular skeleton and remained intact. Concerning the F_{1s} signal, the same two components (as in the starting material) were observed. The component assigned to pentafluorophenolate molecule was decreased after 4 runs of reactions indicating also that it can be washed away from the support along the runs.

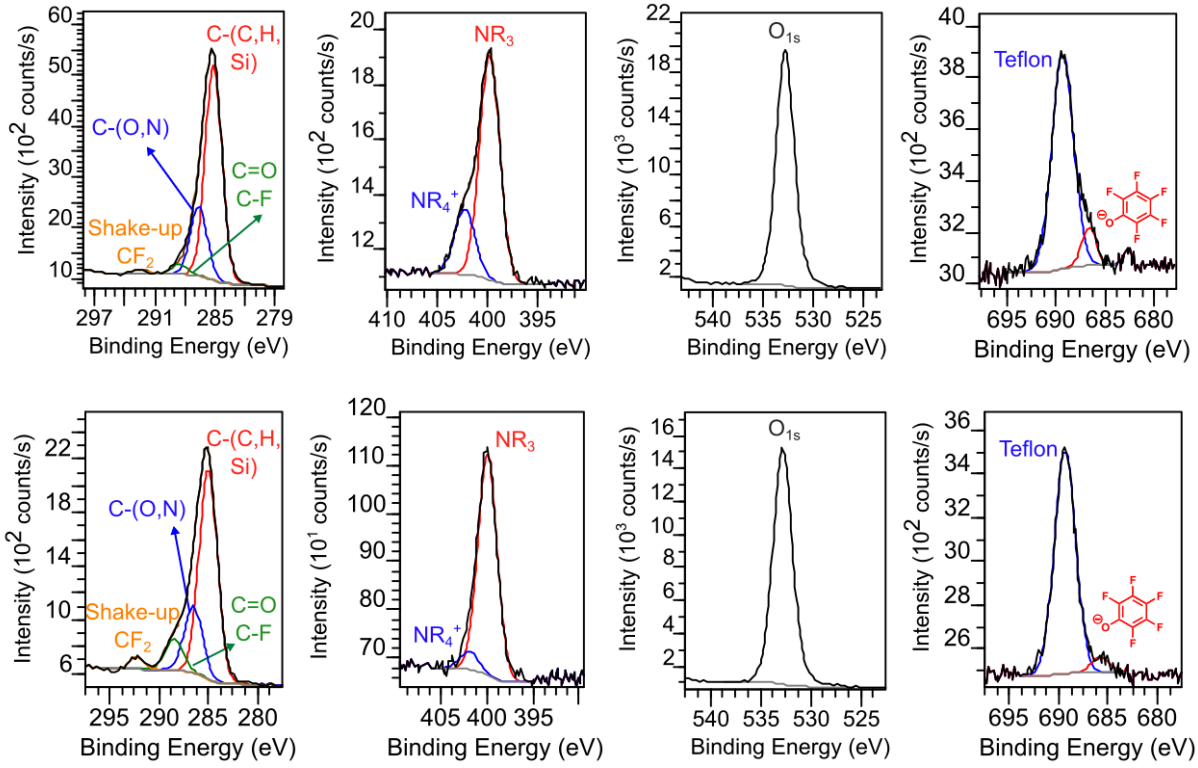

Figure 7. XPS spectra of C_{1s}, N_{1s}, O_{1s} and F_{1s} elements for heterogenized **10a@SiO₂** on silica nanospheres (top) and heterogenized **10a@SiO₂** on silica nanospheres after 4 runs of reaction (bottom).

Our new heterogenized system is competitive with the ones found in the literature. Indeed, porphyrins and methylene blue were immobilized onto silica nanocomposites and were efficient in the photoproduction of singlet oxygen and recyclable over 3 and 4 runs, respectively.[25, 47] The amount of immobilized PS was in the same range as for the porphyrin and methylene blue photosensitizers. Our system is even more efficient than the ones developed by Terra *et al.* for citronellol photooxidation in which Rose Bengal immobilized on magnetic silica nanoparticles showed a drastic decrease in conversion in the first reuse cycle. On the other hand, $[Ru(bpy)_3]^{2+}$ could be used in 3 cycles (85 % conversion) with minimal loss in activity, but at the fifth run the activity dropped to 65 % conversion only.[24a] Our group also highlighted the photobleaching of Rose Bengal immobilized on non-porous silica structures demonstrating a drastic decrease in photoactivity from the first reuse cycle.[24b] In this same work, the use of core-shell silica nanoparticles with a mesoporous shell acted as a shield to reduce the photobleaching of Rose Bengal. This opens future perspectives for fine tuning the present system by playing with the silica nano-structuration and/or loading (for example by decreasing it).

3. CONCLUSIONS

Benzophenazine molecules were easily and diversely functionalized leading to the establishment of a structure-activity relationship by derivatizing three identified zones of the molecular backbone: the southern, the western and the northern fragments. Based on computational results, relevant moieties were identified along with the understanding of the nature of the first excited state.

These results highlighted the probable inertness of the northern fragment on photophysical properties and the different energy transfer mechanisms that can occur depending on the functionalization of the southern fragment. The series of benzophenazines investigated computationally were synthesized easily in two steps from affordable and available starting materials. The photophysical properties, the ability to interact with oxygen and the photostability were assessed. The southern part had a huge impact on the PS activity. Compounds **10a** and sulfur-based derivatives (aromatic or aliphatic sulfur) exhibited great properties such as high phosphorescence lifetimes (~3.5 µs), populated and energetic triplet states, high $^1O_2$ quantum yields (~0.75), efficient citronellol conversion (nearly quantitative) and good photostability. The low ΔE_{ST} and heavy atom effect could explain their amazing efficiencies. Functionalizing the southern fragment with a morpholine moiety led to a peculiar PS with contrasted properties but a good activity in citronellol photooxidation. This was the only nitrogen function that was efficient on the southern part as the others gave poor results and were not efficient in the production of singlet oxygen. The functionalization on the western fragment had no significant impact and was detrimental for certain photophysical properties.

With the nearly inertness of the northern fragment, compound **10a** was advantageously modified and grafted onto silica nanospheres by an amide linker. An activated ester was synthesized to favor the formation of covalent bonds with the amino groups introduced at the surface of the support. XPS and TGA analyses proved the successful anchoring of the PS on the solid particles with a loading of 7.8 wt.% The heterogenized system was performant in the citronellol photooxidation and was robust in recyclability tests as it could be engaged in three recycling runs with only slightly decreased yields. This opens the door for versatile photocatalyst immobilization as our methodology is efficient and involves basic functional groups that can be present on various molecular skeletons and supports. Our supported system could also be employed in different applications such as photodynamic therapy, natural products synthesis, depollution, flow chemistry and the real extent of its potential is still to be discovered.

ASSOCIATED CONTENT

Supporting information. Experimental information, photophysical studies of benzophenazine derivatives, characterization of silica nanospheres, heterogenization studies, computational studies details, and NMR and HRMS spectra.

AUTHOR INFORMATION

Corresponding authors

*Email: sophie.hermans@uclouvain.be; olivier.riant@uclouvain.be

Notes

The authors declare no competing financial interests.

ACKNOWLEDGMENT

NB, SE, L.T.-G. and SH thank the Belgian National Funds for Scientific Research (F.R.S-FNRS) for their Fund for Research Training in Industry and Agriculture (FRIA) PhD Grant (NB and SE), chercheur qualifié position (L.T.-G.) and Research Director position (SH). NB thanks the Région Wallonne for its participation in the FRIA scheme. CL thanks INNOVIRIS for the funding of a BRIDGE project entitled "PhotoCop: Sustainable Photocatalysis with Copper Complexes" (ref: RBC (Région Bruxelles-Capitale)/2019-BRIDGE-5d). The authors thank Pierre Eloy and Jean-François Statsyns for their precious assistance in XPS analyses and the nitrogen physisorption analysis, respectively. Finally, they thank Dr. S. Ouk for his generous financial support through the Fondation Louvain allowing the purchase of a solvents purification system. They are also grateful to Prof. Benjamin Elias and the corresponding grant (no. U.N021.21) for the access to time-resolved photoluminescence spectroscopy.

REFERENCES

[1] M. Hayyan, M. A. Hashim, I. M. AlNashef, *Chem. Rev.* **2016**, *116*, 3029-3085.

[2] a) I. Pyszka, Z. Kucybala, B. Jędrzejewska, *Materials* **2021**, *14*, 3085; b) J. Delaire, J. Pirard, R. Méallet-Renault, G. Clavier, *Photophysique et Photochimie – Des Fondements Aux Applications*, EDP Sciences, **2016**, p. 445-452.

[3] M. C. DeRosa, R. J. Crutchley, *Coord. Chem. Rev.* **2002**, *233*, 351-371.

[4] a) L. Villén, F. Manjón, D. García-Fresnadillo, G. Orellana, *Appl. Catal. B Environ.* **2006**, *69*, 1-9; b) M. E. Jiménez-Hernández, F. Manjón, D. García-Fresnadillo, G. Orellana, *Sol. Energy* **2006**, *80*, 1382-1387; c) R. Bonnett, M. A. Krysteva, I. G. Lalov, S. V. Artarsky, *Water Res.* **2006**, *40*, 1269-1275.

[5] a) X. Xie, Z. Zhang, Y. Hu, H. Cheng, *Chem. Eng. J.* **2018**, *334*, 1242-1251; b) E. Díez-Mato, F. Cortezón-Tamarit, S. Bogialli, D. García-Fresnadillo, M. Marazuela, *Appl. Catal. B Environ.* **2014**, *160-161*, 445-455; c) H. Kim, W. Kim, Y. Mackeyev, G.-S. Lee, H.-J. Kim, T. Tachikawa, S. Hong, S. Lee, J. Kim, L. J. Wilson, T. Majima, P. J. J. Alvarez, W. Choi, J. Lee, *Environ. Sci. Technol.* **2012**, *46*, 9606-9613.

[6] a) I. S. Mfouo-Tynga, L. D. Dias, N. M. Inada, C. Kurachi, *Photodiagnosis Photodyn. Ther.* **2021**, *34*, 102091; b) J. Sandland, R. W. Boyle, *Bioconjug. Chem.* **2019**, *30*, 975–993; c) V. F. Otvagin, N. S. Kuzmina, E. S. Kudriashova, A. V. Nyuchev, A. E. Gavryushin, A. Y. Fedorov, *J. Med. Chem.* **2022**, *65*, 1695–1734; d) J. Li, T. Chen, *Coord. Chem. Rev.* **2020**, *418*, 213355; e) W. Zhang, A. Ahmed, H. Cong, S. Wang, Y. Shen, B. Yu, *Dyes Pigments* **2021**, *185*, 108937; f) S. Moghassemi, A. Dadashzadeh, R. B. Azevedo, O. Feron, C. A. Amorim, *J. Controlled Release* **2021**, *339*, 75–90; g) V.-N. Nguyen, Y. Yan, J. Zhao, J. Yoon, *Acc. Chem. Res.* **2021**, *54*, 207–220; h) D. Chen, Z. Zhong, Q. Ma, J. Shao, W. Huang, X. Dong, *ACS Appl. Mater. Interfaces* **2020**, *12*, 26914–26925.

[7] a) Y. Liu, R. Qin, S. A. Zaat, E. Breukink, M. Heger, *J. Clin. Transl. Res.* **2015**, *1*, 140–167; b) E. Polat, K. Kang, *Biomedicines* **2021**, *9*, 584; c) Q. Han, J. W. Lau, T. C. Do, Z. Zhang, B. Xing, *ACS Appl. Bio Mater.* **2021**, *4*, 3937–3961.

[8] a) D. Kalaitzakis, M. Triantafyllakis, M. Sofiadis, D. Noutsias, G. Vassilikogiannakis, *Angew. Chem.* **2016**, *55*, 4605–4609; b) T. Montagnon, D. Noutsias, I. Alexopoulou, M. Tofi, G. Vassilikogiannakis, *Org. Biomol. Chem.* **2011**, *9*, 2031–2039; c) A. A. Ghogare, A. Greer, *Chem. Rev.* **2016**, *116*, 9994-10034.

[9] C. Michelin, C. Lefebvre, N. Hoffmann, *L'actualité chimique* **2019**, *436*, 1-64.

[10] J. Turconi, F. Griolet, R. Guevel, G. Oddon, R. Villa, A. Geatti, M. Hvala, K. Rossen, R. Göller, A. Burgard, *Org. Process Res. Dev.* **2014**, *18*, 417–422.

[11] a) Q. Zhou, W. Lei, J. Chen, C. Li, Y. Hou, X. Wang, B. Zhang, *Chem. Eur. J.* **2010**, *16*, 3157–3165; b) J. Demas, D. Diemente, E. Harris, *J. Am. Chem. Soc.* **1973**, *95*, 6864–6865; c) K. El-Naggar, H. S. Abdel-Samad, R. M. Ramadan, M. E. El-Khouly, A. A. Abdel-Shafi, *J. Photochem. Photobiol. Chem.* **2023**, *436*, 114405; d) S. P. Foxon, M. A. Alamiry, M. G. Walker, A. J. Meijer, I. V. Sazanovich, J. A. Weinstein, J. A. Thomas, *J. Phys. Chem. A* **2009**, *113*, 12754–12762; e) A. A. Abdel-Shafi, D. R. Worrall, A. Y. Ershov, *Dalton Trans.* **2004**, 30–36.

[12] a) P. I. Djurovich, D. Murphy, M. E. Thompson, B. Hernandez, R. Gao, P. L. Hunt, M. Selke, *Dalton Trans.* **2007**, 3763–3770; b) S. Takizawa, R. Aboshi, S. Murata, *Photochem. Photobiol. Sci.* **2011**, *10*, 895–903; c) D. Ashen-Garry, M. Selke, *Photochem. Photobiol.* **2014**, *90*, 257–274; d) J. Sun, J. Zhao, H. Guo, W. Wu, *Chem. Commun.* **2012**, *48*, 4169–4171.

[13] a) M. G. Kallitsakis, D. K. Gioftsidou, M. A. Tzani, P. A. Angaridis, M. A. Terzidis, I. N. Lykakis, *J. Org. Chem.* **2021**, *86*, 13503–13513; b) M. Rentschler, P. J. Boden, M. A. Argüello Cordero, S. T. Steiger, M.-A. Schmid, Y. Yang, G. Niedner-Schatteburg, M. Karnahl, S. Lochbrunner, S. Tschierlei, *Inorg. Chem.* **2022**, *61*, 12249–12261; c) Y. Yang, F. Doettinger, C. Kleeberg, W. Frey, M. Karnahl, S. Tschierlei, *Front. Chem.* **2022**, *10*, 936863.

[14] a) D. Kalaitzakis, T. Montagnon, E. Antonatou, N. Bardají, G. Vassilikogiannakis, *Chem. Eur. J.* **2013**, *19*, 10119–10123; b) C. Liu, H. Liu, X. Zheng, S. Chen, Q. Lai, C. Zheng, M. Huang, K. Cai, Z. Cai, S. Cai, *ACS Catal.* **2022**, *12*, 1375–1381; c) R. Liu, Q. Liu, H. Meng, H. Ding, J. Hao, Z. Ji, H. Yue, W. Wei, *Org. Chem. Front.* **2021**, *8*, 1970–1975; d) C. Sharma, S. Kumar, N. Jain, *Org. Biomol. Chem.* **2020**, *18*, 2921–2928; e) D. P. Hari, B. König, *Chem. Commun.* **2014**, *50*, 6688–6699.

[15] a) J. Vara, M. S. Gualdesi, S. G. Bertolotti, C. S. Ortiz, *J. Mol. Struct.* **2019**, *1181*, 1–7; b) F. Ronzani, A. Trivella, E. Arzoumanian, S. Blanc, M. Sarakha, C. Richard, E. Oliveros, S. Lacombe, *Photochem. Photobiol. Sci.* **2013**, *12*, 2160–2169.

[16] a) X. Wang, H. Lv, Y. Sun, G. Zu, X. Zhang, Y. Song, F. Zhao, J. Wang, *Spectrochim. Acta. A. Mol. Biomol. Spectrosc.* **2022**, *279*, 121447; b) P. Lo, J. Huang, D. Y. Cheng, E. Y. Chan, W. Fong, W. Ko, D. K. Ng, *Chem. Eur. J.* **2004**, *10*, 4831–4838; c) A. Garai, M. Villa, M. Marchini, S. K. Patra, T. Pain, S. Mondal, P. Ceroni, S. Kar, *Eur. J. Inorg. Chem.* **2021**, *2021*, 4089–4095; d) M. Pineiro, d'A AM, R. Gonsalves, M. M. Pereira, S. J. Formosinho, L. G. Arnaut, *J. Phys. Chem. A* **2002**, *106*, 3787–3795.

[17] a) P. Rana, N. Singh, P. Majumdar, S. P. Singh, *Coord. Chem. Rev.* **2022**, *470*, 214698; b) S. G. Awuah, J. Polreis, V. Biradar, Y. You, *Org. Lett.* **2011**, *13*, 3884–3887; c) M. J. Ortiz, A. R. Agarrabeitia, G. Duran-Sampedro, J. B. Prieto, T. A. Lopez, W. A. Massad, H. A. Montejano, N. A. García, I. L. Arbeloa, *Tetrahedron* **2012**, *68*, 1153–1162; d) N. Adarsh, R. R. Avirah, D. Ramaiah, *Org. Lett.* **2010**, *12*, 5720–5723.

[18] a) A. Pinto, Y. Mace, F. Drouet, E. Bony, R. Boidot, N. Draoui, I. Lobysheva, C. Corbet, F. Polet, R. Martherus, Q. Deraedt, J. Rodríguez, C. Lamy, O. Schicke, D. Delvaux, C. Louis, R. Kiss, A. Kriegsheim, C. Dessy, B. Elias, O. Riant, O. Feron, *Oncogene* **2016**, *35*, 3976–3985; b) K. Ohira, K. Imato, Y. Ooyama, *Mater. Chem. Front.* **2021**, *5*, 5298–5304; c) K. Imato, K. Ohira, M. Yamaguchi, T. Enoki, Y. Ooyama, *Mater. Chem. Front.* **2020**, *4*, 589–596; d) Y. Hayashi, A. Morimoto, T. Maeda, T. Enoki, Y. Ooyama, Y. Matsui, H. Ikeda, S. Yagi, *New J. Chem.* **2021**, *45*, 2264–2275; e) K. Ohira, M. Yamamoto, K. Imato, Y. Ooyama, *New J. Chem.* **2023**, *47*, 2711-2718.

[19] a) S. Lacombe, T. Pigot, *Catal. Sci. Technol.* **2016**, *6*, 1571–1592; b) P. Rana, B. Kaushik, K. Solanki, K. M. Saini, R. Sharma, *Chem. Commun.* **2022**, *58*, 11354–11377.

[20] a) B. M. Estevão, F. Cucinotta, N. Hioka, M. Cossi, M. Argeri, G. Paul, L. Marchese, E. Gianotti, *Phys. Chem. Chem. Phys.* **2015**, *17*, 26804–26812; b) C. Mendoza, N. Emmanuel, C. A. Páez, L. Dreesen, J. M. Monbaliu, B. Heinrichs, *ChemPhotoChem* **2018**, *2*, 890–897; c) C. Mendoza, N. Emmanuel, C. A. Paez, L. Dreesen, J.-C. Monbaliu, B. Heinrichs, *J. Photochem. Photobiol.*

Chem. **2018**, *356*, 193–200; d) M. Lancel, C. Gomez, M. Port, Z. Amara, *Front. Chem. Eng.* **2021**, *3*, 752364; e) J. Xu, T. Pelluau, C. Monnereau, Y. Guari, L. Bonneviot, M. Rodríguez-Pizarro, B. Albela, *New J. Chem.* **2023**, *47*, 1861–1871; f) D. B. Tada, L. L. Vono, E. L. Duarte, R. Itri, P. K. Kiyohara, M. S. Baptista, L. M. Rossi, *Langmuir* **2007**, *23*, 8194–8199; g) L. M. Rossi, P. R. Silva, L. L. Vono, A. U. Fernandes, D. B. Tada, M. S. Baptista, *Langmuir* **2008**, *24*, 12534–12538; h) V. Kabanov, D. J. Press, R. P. Huynh, G. K. Shimizu, B. Heyne, *Chem. Commun.* **2018**, *54*, 6320–6323.

[21] H. Wang, Q. Tang, Z. Chen, T. Li, J. Wang, *Sci. China Mater.* **2020**, *63*, 2189–2205.

[22] a) A. Vinu, K. Z. Hossain, K. Ariga, *J. Nanosci. Nanotechnol.* **2005**, *5*, 347–371; b) F. Hoffmann, M. Cornelius, J. Morell, M. Fröba, *Angew. Chem. Int. Ed.* **2006**, *45*, 3216–3251; c) J. A. S. Costa, R. A. de Jesus, D. O. Santos, J. B. Neris, R. T. Figueiredo, C. M. Paranhos, *J. Environ. Chem. Eng.* **2021**, *9*, 105259; d) R. G. Acres, A. V. Ellis, J. Alvino, C. E. Lenahan, D. A. Khodakov, G. F. Metha, G. G. Andersson, *J. Phys. Chem. C* **2012**, *116*, 6289–6297; e) D. W. Kurka, M. Niehues, S. Kudruk, V. Gerke, B. J. Ravoo, *Chem. Eur. J.* **2021**, *27*, 7667–7676.

[23] I. Rahman, P. Vejayakumaran, C. Sipaut, J. Ismail, C. Chee, *Mater. Chem. Phys.* **2009**, *114*, 328–332.

[24] a) J. C. Terra, A. Desgranges, Z. Amara, A. Moores, *Catal. Today* **2023**, *407*, 52–58; b) N. Body, C. Lefebvre, P. Eloy, T. Haynes, S. Hermans, O. Riant, *J. Photochem. Photobiol. Chem.* **2023**, *440*, 114648; c) J. Flores, P. Moya, F. Bosca, M. L. Marin, *Catal. Today* **2023**, *413–415*, 113994; d) A. Uppal, B. Jain, P. K. Gupta, K. Das, *Photochem. Photobiol.* **2011**, *87*, 1146–1151.

[25] M. Tamtaji, M. Kazemeini, *J. Nanoparticle Res.* **2022**, *24*, 174.

[26] X. Ma, S. Sreejith, Y. Zhao, *ACS Appl. Mater. Interfaces* **2013**, *5*, 12860–12868.

[27] a) J. Wahlen, D. E. De Vos, P. A. Jacobs, P. L. Alsters, *Adv. Synth. Catal.* **2004**, *346*, 152–164; b) C. H. Mak, X. Han, M. Du, J.-J. Kai, K. F. Tsang, G. Jia, K.-C. Cheng, H.-H. Shen, H.-Y. Hsu, *J. Mater. Chem. A* **2021**, *9*, 4454–4504.

[28] a) Y. Guo, S. Rogelj, P. Zhang, *Nanotechnology* **2010**, *21*, 065102; b) E. Gianotti, B. Martins Estevão, F. Cucinotta, N. Hioka, M. Rizzi, F. Renò, L. Marchese, *Chem. Eur. J.* **2014**, *20*, 10921–10925.

[29] a) S. Kothavale, N. Sekar, *Dyes Pigments* **2017**, *136*, 31–45; b) B. C. Raju, K. V. Prasad, G. Saidachary, B. Sridhar, *Org Lett* **2014**, *45*, 420–423; c) P. Singh, A. Baheti, K. J. Thomas, *J. Org. Chem.* **2011**, *76*, 6134–6145; d) A. K. Mishra, J. N. Moorthy, *J. Org. Chem.* **2016**, *81*, 6472–6480.

[30] a) N. Trempolec, B. Doix, C. Degavre, D. Brusa, C. Bouzin, O. Riant, O. Feron, *Cancers* **2020**, *12*, 545; b) B. Doix, N. Trempolec, O. Riant, O. Feron, *Front. Oncol.* **2019**, *9*, 811; c) B. Doix, E. Bastien, A. Rambaud, A. Pinto, C. Louis, V. Grégoire, O. Riant, O. Feron, *Front. Oncol.* **2018**, *8*, 393; d) S. Moghassemi, A. Dadashzadeh, A. Camboni, O. Feron, R. B. Azevedo, C. A. Amorim, *Photodiagnosis Photodyn. Ther.* **2022**, *40*, 103139; e) S. Moghassemi, A. Dadashzadeh, A. Camboni, O. Feron, R. B. Azevedo, C. A. Amorim, *Hum. Reprod. Open* **2023**, *2023*, hoad005.

[31] a) S. Jiménez-Alonso, H. C. Orellana, A. Estevez-Braun, A. G. Ravelo, E. Perez-Sacau, F. Machin, *J. Med. Chem.* **2008**, *51*, 6761–6772; b) E. Pérez-Sacau, R. G. Díaz-Peñate, A. Estévez-Braun, A. G. Ravelo, J. M. García-Castellano, L. Pardo, M. Campillo, *J. Med. Chem.* **2007**, *50*, 696–706; c) V. F. de Andrade-Neto, M. O. Goulart, J. F. da Silva Filho, M. J. Da Silva, F. Maria do Carmo, A. V. Pinto, M. G. Zalis, L. H. Carvalho, A. U. Krettli, *Bioorg. Med. Chem. Lett.* **2004**, *14*, 1145–1149.

[32] A. B. Tathe, N. Sekar, *J. Fluoresc.* **2015**, *25*, 1403–1415.

[33] D. Jacquemin, V. Wathelet, E. A. Perpete, C. Adamo, *J. Chem. Theory Comput.* **2009**, *5*, 2420–2435.

[34] F. Weigend, R. Ahlrichs, *Phys. Chem. Chem. Phys.* **2005**, *7*, 3297–3305.

[35] M. J. Frisch, G. W. Trucks, H. B. Schlegel, G. E. Scuseria, M. Robb, J. R. Cheeseman, G. Scalmani, V. Barone, G. A. Petersson, H. Nakatsuji *et al.*, *Gaussian 16*, Gaussian Inc, Wallingford CT, **2016.**

[36] Z. Liu, T. Lu, Q. Chen, *Carbon* **2020**, *165*, 461–467.
[37] E. D. Glendening, C. R. Landis, F. Weinhold, *J. Comput. Chem.* **2019**, *40*, 2234–2241.
[38] M. J. Hatfield, J. Chen, E. M. Fratt, L. Chi, J. C. Bollinger, R. J. Binder, J. Bowling, J. L. Hyatt, J. Scarborough, C. Jeffries, P. M. Potter, *J. Med. Chem.* **2017**, *60*, 1568–1579.
[39] A. Rodriguez-Serrano, V. Rai-Constapel, M. C. Daza, M. Doerr, C. M. Marian, *Phys Chem Chem Phys* **2015**, *17*, 11350.
[40] a) P. de Silva, *J Phys Chem Lett* **2019**, *10*, 5674–5679; b) R. Pollice, P. Friederich, C. Lavigne, G. dos Passos Gomes, A. Aspuru-Guzik, *Matter* **2021**, *4*, 1654–1682; c) J. Ehrmaier, E. J. Rabe, S. R. Pristash, K. L. Corp, C. W. Schlenker, A. L. Sobolewski, W. Domcke, *J Phys Chem A* **2019**, *123*, 8099–8108.
[41] E. Pang, S. Zhao, B. Wang, G. Niu, X. Song, M. Lan, *Coord. Chem. Rev.* **2022**, *472*, 214780.
[42] C. M. Marian, *Wiley Interdiscip. Rev. Comput. Mol. Sci.* **2012**, *2*, 187–203.
[43] M. Dichiara, O. Prezzavento, A. Marrazzo, V. Pittala, L. Salerno, A. Rescifina, E. Amata, *Eur. J. Med. Chem.* **2017**, *142*, 459–485.
[44] T. Entradas, S. Waldron, M. Volk, *J. Photochem. Photobiol. B* **2020**, *204*, 111787.
[45] a) I. K. Mbaraka, B. H. Shanks, *J. Am. Oil Chem. Soc.* **2006**, *83*, 79–91; b) C. G. Thomson, A.-L. Lee, F. Vilela, *Beilstein J. Org. Chem.* **2020**, *16*, 1495–1549; c) V. Vattipalli, X. Qi, P. J. Dauenhauer, W. Fan, *Chem. Mater.* **2016**, *28*, 7852–7863; d) A. A. Kiss, A. C. Dimian, G. Rothenberg, *Adv. Synth. Catal.* **2006**, *348*, 75–81; e) V.-T. Hoang, Q. Huang, M. Eić, T.-O. Do, S. Kaliaguine, *Langmuir* **2005**, *21*, 2051–2057.
[46] W. Stöber, A. Fink, E. Bohn, *J. Colloid Interface Sci.* **1968**, *26*, 62–69.
[47] S. M. Ribeiro, A. C. Serra, A. d'A R. Gonsalves, *J. Mol. Catal. Chem.* **2010**, *326*, 121–127.